AIAA JOURNAL
Vol. 46, No. 2, February 2008

Robustness Analysis and Robust Design of Uncertain Systems

Luis G. Crespo*
National Institute of Aerospace, Hampton, Virginia 23666
and
Daniel P. Giesy† and Sean P. Kenny‡
NASA Langley Research Center, Hampton, Virginia 23681

DOI: 10.2514/1.28683

This paper proposes a methodology for the analysis and design of systems subject to parametric uncertainty in which design requirements are specified via hard inequality constraints. Hard constraints are those that must be satisfied for all parameter realizations within a given uncertainty model. Uncertainty models given by norm-bounded perturbations from a nominal parameter value (i.e., hyperspheres) and by sets of independently bounded uncertain variables (i.e., hyperrectangles) are the focus of this paper. These models, which are also quite practical, allow for a rigorous mathematical treatment within the proposed framework. Hard-constraint feasibility is determined by sizing the largest uncertainty set for which the design requirements are satisfied. Assessments of robustness are attained by comparing this set with the actual uncertainty model. These assessments do not suffer from the numerical deficiencies of sampling-based methods. Strategies that enable the comparison of the robustness characteristics of competing design alternatives, the approximation of the robust design space, and the systematic search for designs with improved robustness are also proposed. Because the problem formulation is generic and the tools derived only require standard optimization algorithms for their implementation, this methodology is applicable to a broad range of engineering problems.

I. Introduction

DESIGN under uncertainty arises in numerous disciplines including engineering, economics, finance and management. Achieving balance between robustness and performance is one of the fundamental challenges faced by scientists and engineers. Tradeoffs must be made to reach acceptable levels of performance with adequate robustness to uncertainty.

Literature in stochastic programming [1] and stochastic approximations [2] with applications to structural safety [3,4] and probabilistic controls [5] provides several mathematical tools for optimization under uncertainty. The algorithms at our disposal can be classified according to the way they enforce inequality constraints that depend on the uncertain parameters. *Hard constraints* [6–10] are those that, for a given uncertainty model, must be satisfied for all possible realizations of the uncertain parameter (a realization is any possible parameter value within the uncertainty model). Strategies to solve this class of optimization problems usually require nested searches in which approximations to the worst-parameter realization [6,11] are made in an inner optimization loop with a growing number of constraints that depend on this approximation sequentially added to the outer loop. These strategies, however, not only become computationally intractable for uncertain parameter vectors of large dimension; but, more important, are unable to provide guarantees of constraint satisfaction. On the other hand, *soft constraints* are those that can be violated by some parameter realizations. Chance-constrained programming [1], sampling-based techniques [12–14], asymptotic approximations [5,15], and penalty-based optimization [1,10] are some of the strategies commonly used to handle soft constraints. Even though this paper concentrates on inequality constraints, equality [16,17] constraints are an integral part of robust design optimization [18–20] strategies.

Some questions arise as to whether it is more appropriate to use hard or soft constraints as design criteria. We agree that at certain stages of design, particularly at conceptual design stage, many of the requirements are fluid in nature and are subject to many levels of tradeoffs. However, as designs evolve outside of the concept stage into implementation, many of the requirements get "locked in" (post-requirements-definition phase of system design) and designers are no longer free to perform gross design trades, as is typically done in conceptual design. This is certainly not against common practice in the aerospace industry. This is not to say that, in the presence of uncertainty, some requirements will eventually need to be relaxed so that overall mission objectives can be achieved. However, this does not imply that every analyst at any stage of the design and analysis would be given freedom to interpret requirements in a "soft" manner. Quite the opposite is the case. Design requirements are almost always prescribed as "must not exceed," or "must be less than." One will rarely see critical mission performance criteria listed as "should not exceed" or "should be less than."

For high-risk decisions, the achievement and verification of strict constraint feasibility are crucial tasks. This paper addresses these needs by developing a methodology for robustness analysis and robust design based on the calculation of certain indicators, called *critical parameter values* and *parametric safety margins* (PSMs). Once the uncertainty model of the input and the functional relation between inputs and outputs are prescribed, the uncertainty model of the output is completely determined. Characterizing this model is not an easy task when the functional relationship is nonlinear, because the output uncertainty set may be nonconvex and multiply connected. For these reasons, most of the uncertainty propagation tools available rely on sampling the uncertainty model of the input, propagating every sample through the function, and studying the ensemble of output samples as a whole. If the function is expensive to evaluate, accurate estimation of this ensemble rapidly becomes unaffordable. This paper proposes an alternative approach for the

Presented as Paper 7035 at the 11th AIAA/ISSMO Multidisciplinary Analysis and Optimization Conference, Portsmouth, VA, 6–8 September 2006; received 2 November 2006; revision received 19 September 2007; accepted for publication 5 October 2007.

*Staff Scientist, 100 Exploration Way; Luis.G.Crespo@nasa.gov. Professional Member AIAA.

†Aerospace Technologist, Mathematician, Dynamic Systems and Control Branch, Research and Technology Directorate, Mail Stop 308; Daniel.P.Giesy@nasa.gov.

‡Aerospace Technologist, Dynamic Systems and Control Branch, Research and Technology Directorate, Mail Stop 308; Sean.P.Kenny@nasa.gov.

characterization of uncertainty in the output, greatly alleviating the computational burden associated with sampling-based methods. The tools developed are based on the numerical solution to an optimization problem for which the only numerical pitfall is the question of whether the optimization has converged to its global optimal. The reference by Crespo et al. [21] supports the developments to be presented herein. Robust design optimization strategies using probabilistic uncertainty models based on the deformation of uncertainty sets have also been recently developed by the authors [22]. Such developments are a natural extension to this paper.

There are similarities between the present approach and the information-gap decision theory developed by Ben-Haim [23–25], in which info-gap uncertainty models are proposed and used for analysis, planning, and design under uncertainty. The info-gap theory is based on two decision functions, called the robustness function and the opportunity function. The robustness function has the same rationale as the similitude ratio of the deformations introduced in this paper. However, the developments herein enable us to consider independent sources of uncertainty, having varying levels of fidelity, and nonlinear parameter dependencies; cases in which the response set may not even admit an info-gap uncertainty model.

This paper is organized as follows. An overview of the content is introduced first. This is followed by the motivation and introduction of the mathematical framework. Tests of robustness and extensions to robust design follow. Two simple examples are used to illustrate the scope of the methods proposed. A few concluding remarks close the paper.

II. Overview

The concern in this paper is the robustness analysis and robust design of a system described by a parametric mathematical model. The parameters that specify the system are grouped into two categories: uncertain parameters, which are denoted by the vector $\boldsymbol{p}$, and design parameters, which are denoted by the vector $\boldsymbol{d}$.

It is assumed that the true unknown value of $\boldsymbol{p}$ lies within the support set, which is the uncertainty model of $\boldsymbol{p}$. In practice, the choice of this model is usually made by a discipline expert, who can use experimental data and engineering judgment (i.e., physical intuition and the experience gained when solving similar problems) to prescribe it. However, the theory presented herein acknowledges that such a choice may be fairly arbitrary and addresses the need for quantifying the level of tolerance of the system to uncertainty in $\boldsymbol{p}$ when a particular $\boldsymbol{d}$ is chosen.

For analysis purposes, $\boldsymbol{d}$ is assumed to take on a fixed value, and for design purposes, $\boldsymbol{d}$ is to be chosen. The design requirements for the system are prescribed by a collection of constraint functions that, in general, depend on both the uncertain and design parameters. The system is deemed acceptable if all constraint functions are satisfied. For each value of the design parameter, these constraint functions partition the uncertain parameter space into two regions: a failure region, in which at least one of the design requirements is not satisfied, and its complement, a safe region in which all requirements are satisfied.

One of the tasks of interest is to assign a measure of robustness to a design point based on measuring how much the support set can be expanded without encroaching on the failure region. This requires specifying what we mean by deforming the support set. Let the *designated point* be an interior point of the support set to be used as an anchor for such deformations. A deformation by a factor of α can be viewed in the following way. Imagine standing at the designated point and looking at any other point of the support set. Denote the distance from the designated point to the other point by δ. A *homothetic* [21] deformation is attained by looking in the same direction and placing the point at a distance of $\alpha\delta$ from the designated point. Expansions are accomplished when $\alpha > 1$ and contractions result from using $\alpha < 1$. In this paper, deformations must be interpreted as homothetic expansions or contractions. Illustrations of homothetic deformation are given in Figs. 1 and 2. In each figure, the

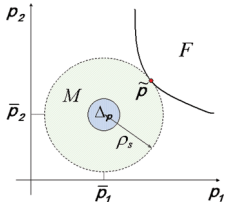

Fig. 1 Relevant metrics for a circular support set.

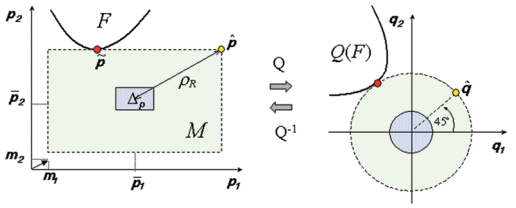

Fig. 2 Relevant metrics for a rectangular support set.

set M results from homothetically deforming the set Δ_p. In the process, orientation and proportionality (in Fig. 2, the aspect ratio of M and Δ_p are equal) are preserved.

For hyperspherical and hyperrectangular uncertainty models, we cast the problem of finding the maximal deformed set fully contained in the safe region, called the *maximal feasible set*, in terms of an optimization problem to which standard nonlinear constrained optimization algorithms are applicable. The robustness of the corresponding design point is proportional to the size of such a set.

The failure domain changes with the design point. For each different design point, a measure of robustness can be calculated. One can then search for a design that admits the largest deformation of the support set. We show how to cast this search in the form of a nonlinear optimization problem. The mathematical groundwork for implementing these ideas is presented next.

III. Framework

Let the *support set*, denoted hereafter as $\Delta_p \subset \mathbb{R}^{\dim(p)}$, be the *uncertainty model* of the uncertain parameter vector $\boldsymbol{p}$. A *realization* of the uncertain parameter is any member of the support set.

The *designated point* $\bar{\boldsymbol{p}} \in \Delta_p$ is an interior point of the support set, that can be considered a good representation of the uncertain parameter. A natural choice for the designated point $\bar{\boldsymbol{p}}$ is the geometric center of Δ_p. One possible choice for the support set is a hypersphere. The hypersphere of radius R centered at $\bar{\boldsymbol{p}}$, denoted as $S_p(\bar{\boldsymbol{p}}, R)$, is defined by

$$S_p(\bar{\boldsymbol{p}}, R) = \{\boldsymbol{p}\colon \|\bar{\boldsymbol{p}} - \boldsymbol{p}\| \le R\} \tag{1}$$

This geometry implies that an arbitrary, norm-bounded perturbation from $\bar{\boldsymbol{p}}$ is a possible value of the uncertain parameter.[§]

Another possible choice might be to confine each component of $\boldsymbol{p}$ to a bounded interval. This is especially desirable when the levels of uncertainty in $\boldsymbol{p}$ are dissimilar. This leads to the choice of Δ_p as a hyperrectangle. If $\boldsymbol{m}$ is the vector of half-lengths of the sides of the rectangle, the hyperrectangle $R_p(\bar{\boldsymbol{p}}, \boldsymbol{m})$ is defined by

$$R_p(\bar{\boldsymbol{p}}, \boldsymbol{m}) = \{\boldsymbol{p}\colon \bar{\boldsymbol{p}} - \boldsymbol{m} \le \boldsymbol{p} \le \bar{\boldsymbol{p}} + \boldsymbol{m}\} \tag{2}$$

Note that here and subsequently, vector inequalities must be satisfied by every component.

[§]There are applications in which uncertainty sets with this geometry are used. For instance, in control theory, there is the μ-analysis and synthesis approach (a popular method for robust controls), in which model form uncertainty on the system dynamics is modeled with norm-bounded perturbations from the nominal plant. Such a model is parameterized even though the parameters are not physical quantities. Additionally, the hypersphere can be used as a support set when the uncertain parameters are nondimensionalized and normalized, as is done in the example in Sec. VI.B.

Note that this geometry allows for the manipulation of sets of parameters having dissimilar levels of uncertainty by making $\boldsymbol{m}_i$ proportional to the level of uncertainty in $\boldsymbol{p}_i$.

Now consider the situation that a system depends on an uncertain parameter $\boldsymbol{p}$ and a design variable $\boldsymbol{d} \in \mathbb{R}^{\dim(\boldsymbol{d})}$. Suppose that

$$\boldsymbol{g}: \mathbb{R}^{\dim(\boldsymbol{p})} \times \mathbb{R}^{\dim(\boldsymbol{d})} \to \mathbb{R}^{\dim(\boldsymbol{g})}$$

is a set of constraint functions on the system, which have been normalized so that positive values represent constraint violations. If these are considered hard constraints, the system corresponding to given values of $\boldsymbol{d}$ and Δ_p will be judged acceptable if

$$\boldsymbol{g}(\boldsymbol{p}, \boldsymbol{d}) \leq \boldsymbol{0} \quad \forall\ \boldsymbol{p} \in \Delta_p$$

The *failure region*, denoted as $F(\boldsymbol{d}, \boldsymbol{g}) \subset \mathbb{R}^{\dim(\boldsymbol{p})}$, is composed of the parameters that do not satisfy all the constraints. Specifically, the failure region for the design point $\boldsymbol{d}$ is given by

$$F(\boldsymbol{d}, \boldsymbol{g}) = \bigcup_{i=1}^{\dim(\boldsymbol{g})} F_i(\boldsymbol{d}, \boldsymbol{g}) \tag{3}$$

where, for $1 \leq i \leq \dim(\boldsymbol{g})$,

$$F_i(\boldsymbol{d}, \boldsymbol{g}) = \{\boldsymbol{p}: \boldsymbol{g}_i(\boldsymbol{p}, \boldsymbol{d}) > 0\} \tag{4}$$

The design $\boldsymbol{d}$ is *robust* if $F(\boldsymbol{d}, \boldsymbol{g})$ and Δ_p do not overlap. Otherwise, $\boldsymbol{d}$ is *nonrobust*. In the former case, the degree of robustness can be quantified by measuring the separation between the two sets.

For purposes of this paper, two uncertainty sets will be called *proportional* if one of the two can be formed by homothetically deforming the other one about a common designated point. This deformation can be seen as an expansion or contraction by some positive factor. Call such a factor the *similitude ratio* and denote it by α. For instance, the hyperrectangles $R_p(\bar{\boldsymbol{p}}, \boldsymbol{m})$ and $R_p(\bar{\boldsymbol{p}}, \alpha\boldsymbol{m})$ are proportional sets.

The notions of critical parameter value and PSM are now introduced. For clarity, the presentation of the material will concentrate on the case in which $\boldsymbol{g}(\bar{\boldsymbol{p}}, \boldsymbol{d}) \leq 0$. The converse case is considered in Sec. IV.D. Intuitively, one imagines that the support set of the uncertainty model is being expanded homothetically with respect to its designated point until its boundary just touches the boundary of the failure region. The points at which the deformed set touches the failure region are the critical parameter values. The maximal feasible set, denoted hereafter as M, is the resulting deformed set. The *critical similitude ratio*, denoted as $\tilde{\alpha}$, is the similitude ratio leading to M, and the PSM to be defined is a metric that quantifies the size of the maximal feasible set. Both the critical similitude ratio and the PSM, provide a measure of robustness of a design to parameter uncertainty. The larger they are, the larger the variation from the designated point to which the uncertain parameter can be subjected without encountering a constraint violation. The critical similitude ratio is nondimensional, but depends on both the shape and the size of the support set. The PSM has the same units as the uncertain parameters and depends on the shape, but not the size, of the set. The mathematical background for these notions is presented next.

Denote by ∂ the set boundary operator.[¶] Let $\boldsymbol{d}$ be a given design and let Δ_p, $\bar{\boldsymbol{p}}$, and $\boldsymbol{g}$ be prescribed in advance. Any $\tilde{\boldsymbol{p}}$ lying in $M \cap \partial F$ will be a critical parameter value for this design, uncertainty model, and constraint set. Note that the critical parameter value might not be a realization of the uncertain parameter; that is, $\tilde{\boldsymbol{p}}$ might not belong to Δ_p. Further note that there may be several critical parameter values.

A design point is deemed to be in the *feasible design space* if it satisfies all the constraints when the uncertain parameter assumes the value of the designated point. The *robust design space* is the set of designs satisfying all the constraints for all members of the support set. Each member of the robust design space set is a robust design. Note that if the robust design space exists, it is a subset of the feasible design space. Formal definitions of the PSMs for hyperspherical and hyperrectangular supports are provided in Sec. IV, as are expressions for the calculation of the critical parameter values. The PSM is proportional to the degree of robustness of $\boldsymbol{d}$ to uncertainty in $\boldsymbol{p}$. If the PSM assumes the value of zero, there is no robustness, because at least one of the constraints is active for $\bar{\boldsymbol{p}}$; that is, because $\bar{\boldsymbol{p}}$ is on the boundary of the failure region, there exist arbitrarily small perturbations from $\bar{\boldsymbol{p}}$, leading to a constraint violation. The convention is that designs within the feasible design space assume nonnegative PSM values; otherwise, they are negative.

IV. Robustness Analysis

Problem Statement: Does the design $\boldsymbol{d}$ satisfy the constraints $\boldsymbol{g}(\boldsymbol{p}, \boldsymbol{d}) \leq 0$ for all $\boldsymbol{p} \in \Delta_p$?

Robustness tests for hyperspherical and hyperrectangular support sets are considered next. These strategies are then used to handle supports with other geometries. In what follows, we assume that $\partial F_j = \{\boldsymbol{p}: \boldsymbol{g}_j(\boldsymbol{p}, \boldsymbol{d}) = 0\}$ for $1 \leq j \leq \dim(\boldsymbol{g})$.

A. Hyperspheres

Hyperspherical support sets result from uncertainty models in which uncertainty is described by norm-bounded perturbations from the nominal parameter value $\bar{\boldsymbol{p}}$. This implies that Δ_p is a hypersphere and $\bar{\boldsymbol{p}}$ is its geometric center. Problems with this class of support sets are the simplest, because the critical parameter value is calculated by solving a set of minimum norm problems in $\boldsymbol{p}$ space. The critical parameter value, denoted hereafter as $\tilde{\boldsymbol{p}}$ for $\Delta_p = S_p(\bar{\boldsymbol{p}}, R)$ when $\boldsymbol{g}(\bar{\boldsymbol{p}}, \boldsymbol{d}) \leq \boldsymbol{0}$, is a $\boldsymbol{p}$ value on the surface of the failure region that minimizes $\|\boldsymbol{p} - \bar{\boldsymbol{p}}\|$; that is,

$$\tilde{\boldsymbol{p}} = \text{argmin}_p\{\|\boldsymbol{p} - \bar{\boldsymbol{p}}\|: \boldsymbol{p} \in \partial F\} \tag{5}$$

This optimization problem is restated[**] as

$$\tilde{\boldsymbol{p}} = \tilde{\boldsymbol{p}}^i \tag{6}$$

where

$$i = \text{argmin}_{1 \leq j \leq \dim(\boldsymbol{g})}\{\|\tilde{\boldsymbol{p}}^j - \bar{\boldsymbol{p}}\|\} \tag{7}$$

and

$$\tilde{\boldsymbol{p}}^j = \text{argmin}_p\{\|\boldsymbol{p} - \bar{\boldsymbol{p}}\|: \boldsymbol{g}_j(\boldsymbol{p}, \boldsymbol{d}) = 0\} \tag{8}$$

Hence, the critical parameter value problem is solved for each individual constraint function, and the answer is selected that is closest to the designated point. Note that the equality constraint in Eq. (8) is a particular case of $\boldsymbol{p} \in \partial F_j$. Assuming that the constraint functions $\boldsymbol{g}$ are continuous, the problem at hand is turned into an "inequality-constraint-only" optimization problem, which is more "optimizer-friendly," by changing the constraint on $\boldsymbol{g}_j$ from $\boldsymbol{g}_j = 0$ to $\boldsymbol{g}_j \geq 0$ because the optimum must occur on ∂F.

The *spherical PSM* corresponding to the design $\boldsymbol{d}$ for $\Delta_p = S_p(\bar{\boldsymbol{p}}, R)$ is defined as

$$\rho_S(\bar{\boldsymbol{p}}, \tilde{\boldsymbol{p}}, \boldsymbol{d}) \stackrel{\Delta}{=} \gamma\|\tilde{\boldsymbol{p}} - \bar{\boldsymbol{p}}\| \tag{9}$$

where γ is equal to 1 if $\boldsymbol{g}(\bar{\boldsymbol{p}}, \boldsymbol{d}) \leq \boldsymbol{0}$ and equal to -1 otherwise. This constant applies the sign convention introduced earlier. Note that $\rho_S = \tilde{\alpha}R$ and the maximal feasible set is $M = S_p(\bar{\boldsymbol{p}}, \rho_S)$. A sketch showing relevant quantities is displayed in Fig. 1. A simple robustness test for hyperspherical supports sets can now be formulated.

[¶]If A is a set, ∂A is the set of all boundary points of A, which means that $x \in \partial A$ if and only if every neighborhood of x touches both A and its complement.

[**]Although vector subscripts will be used to denote vector components, superscripts will be used to denote particular vectors; for example, $\boldsymbol{p}_j^i$ is the jth component of the vector $\boldsymbol{p}^i$.

P-test: The design $\boldsymbol{d}$ satisfies the hard constraints prescribed by $\Delta_p = S_p(\bar{\boldsymbol{p}}, R)$ and $\boldsymbol{g}(\boldsymbol{p}, \boldsymbol{d}) \leq \boldsymbol{0}$ if and only if $\rho_S \geq R$. This condition is equivalent to $\tilde{\alpha} \geq 1$.

The robust design space corresponding to $\Delta_p = S_p(\bar{\boldsymbol{p}}, R)$ is given by $\{\boldsymbol{d}\colon \rho_S \geq R\}$, for which the boundary is the iso-spherical PSM manifold $\rho_S(\boldsymbol{d}) = R$.

B. Hyperrectangles

Recall that if $\bar{\boldsymbol{p}}$ is the geometric center of the hyperrectangle and $\boldsymbol{m}$ is the vector of half-lengths of its sides, the resulting hyperrectangle is denoted as $R_p(\bar{\boldsymbol{p}}, \boldsymbol{m})$. A robustness test for supports with this geometry is introduced in this section. The mathematical background for this is presented next.

1. Q-Transformation

Let $\Delta_p = R_p(\bar{\boldsymbol{p}}, \boldsymbol{m})$ be the support of $\boldsymbol{p}$. The *Q-transformation*, denoted as $\boldsymbol{q} = Q(\boldsymbol{p})$, is given by

$$\boldsymbol{q} \triangleq \frac{\max\{|\boldsymbol{k}|\}\boldsymbol{k}}{\|\boldsymbol{k}\|} \tag{10}$$

where

$$\boldsymbol{k} = \operatorname{diag}\{\boldsymbol{m}\}^{-1}(\boldsymbol{p} - \bar{\boldsymbol{p}}) \tag{11}$$

The corresponding inverse transformation $\boldsymbol{p} = Q^{-1}(\boldsymbol{q})$ is given by

$$\boldsymbol{p} = \bar{\boldsymbol{p}} + \frac{\|\boldsymbol{q}\|\operatorname{diag}\{\boldsymbol{m}\}\boldsymbol{q}}{\max\{|\boldsymbol{q}|\}} \tag{12}$$

The Q-transformation transforms $R_p(\bar{\boldsymbol{p}}, \boldsymbol{m})$ into a unit hypersphere in $\boldsymbol{q}$ space centered at the origin. Q maps sets proportional to the hyperrectangle to sets proportional to the hypersphere while preserving the similitude ratio:

$$Q[R_p(\bar{\boldsymbol{p}}, \alpha\boldsymbol{m})] = S_q(\boldsymbol{0}, \alpha) \tag{13}$$

Notice that the Q-transformation introduces derivative discontinuities. These discontinuities occur at points corresponding to $\boldsymbol{p}$-space points at which the faces of hyperrectangles proportional to the support set meet.

The Q-transformation enables the easy manipulation of hyperrectangular sets (e.g., sampling their volumes, surfaces, and determining if a given $\boldsymbol{p}$ is within the set). More important, it allows the identification of the corresponding critical parameter value by solving a set of minimum norm problems in $\boldsymbol{q}$ space. Specifically, when $\boldsymbol{g}(\bar{\boldsymbol{p}}, \boldsymbol{d}) \leq \boldsymbol{0}$, the critical parameter value can be found by solving

$$\tilde{\boldsymbol{p}} = \tilde{\boldsymbol{p}}^i \tag{14}$$

where

$$i = \operatorname{argmin}_{1 \leq j \leq \dim(\boldsymbol{g})}\{\|Q(\tilde{\boldsymbol{p}}^j)\|\} \tag{15}$$

and

$$\tilde{\boldsymbol{p}}^{\,j} = \operatorname{argmin}_{\boldsymbol{p}}\{\|Q(\boldsymbol{p})\|\colon \boldsymbol{g}_j(\boldsymbol{p}, \boldsymbol{d}) = 0\} \tag{16}$$

Hence, the critical parameter value problem is solved for each individual constraint function, and the answer is the one for which the norm in $\boldsymbol{q}$ space is the smallest. As before, properties of the critical parameter value allow us to replace the equality constraint with an inequality constraint.

The *rectangular PSM* corresponding to the design $\boldsymbol{d}$ for $\Delta_p = R_p(\bar{\boldsymbol{p}}, \boldsymbol{m})$ is defined as

$$\rho_R(\bar{\boldsymbol{p}}, \tilde{\boldsymbol{p}}, \boldsymbol{m}, \boldsymbol{d}) \triangleq \gamma \left\| Q^{-1}\left(\frac{\|Q(\tilde{\boldsymbol{p}})\| \cdot \boldsymbol{1}}{\sqrt{\dim(\boldsymbol{p})}}\right) - \bar{\boldsymbol{p}} \right\| \tag{17}$$

where $\boldsymbol{1}$ is a vector of ones and γ was defined following Eq. (9). Note that this expression is equivalent to $\tilde{\alpha}\|\boldsymbol{m}\|$. The corresponding maximal feasible set is given by $M = R_p(\bar{\boldsymbol{p}}, \rho_R \boldsymbol{m}/\|\boldsymbol{m}\|)$. As always, M is the largest set proportional to Δ_p that contains no constraint-violation points.

A sketch showing relevant quantities is displayed in Fig. 2. Note that $\hat{\boldsymbol{p}} = \bar{\boldsymbol{p}} + \tilde{\alpha}\boldsymbol{m}$ and $\hat{\boldsymbol{q}} = Q(\hat{\boldsymbol{p}})$. The rectangular PSM is related to the diagonal measure of this hyperrectangle. This provides comparability between rectangular PSMs measured, for example, for different design points and therefore different constraint geometries and different locations of the critical parameter value. Note that M is inscribed in a hypersphere centered at $\bar{\boldsymbol{p}}$ of a radius equal to its rectangular PSM.

2. Infinity Norm Formulation

An alternative way to search for the critical parameter value for hyperrectangular supports is presented here. This formulation allows us to circumvent the problems caused by discontinuities in the gradient of the Q-transformation.

Recall that the infinity norm in a finite dimensional space is defined as $\|\boldsymbol{x}\|^\infty = \sup_i\{|\boldsymbol{x}_i|\}$. Let us define the $\boldsymbol{m}$-scaled infinity norm as $\|\boldsymbol{x}\|_{\boldsymbol{m}}^\infty = \sup_i\{|\boldsymbol{x}_i|/\boldsymbol{m}_i\}$. A distance between the vectors $\boldsymbol{x}$ and $\boldsymbol{y}$ can be defined as $\|\boldsymbol{x} - \boldsymbol{y}\|_{\boldsymbol{m}}^\infty$. Using this distance, the unit ball centered at $\bar{\boldsymbol{p}}$ is just $R(\bar{\boldsymbol{p}}, \boldsymbol{m})$.

In this context, the critical parameter value for the vector of constraints $\boldsymbol{g}(\boldsymbol{p}, \boldsymbol{d}) \leq 0$ and for the uncertainty model given by $R(\bar{\boldsymbol{p}}, \boldsymbol{m})$ and $\bar{\boldsymbol{p}}$ results from using the $\boldsymbol{m}$-scaled infinity norm in Eq. (5). This optimization problem is restated as

$$\tilde{\boldsymbol{p}} = \tilde{\boldsymbol{p}}^i \tag{18}$$

where

$$i = \operatorname{argmin}_{1 \leq j \leq \dim(\boldsymbol{g})}\left\{\|\tilde{\boldsymbol{p}}^j - \bar{\boldsymbol{p}}\|_{\boldsymbol{m}}^\infty\right\} \tag{19}$$

and

$$\tilde{\boldsymbol{p}}^{\,j} = \operatorname{argmin}_{\boldsymbol{p}}\left\{\|\boldsymbol{p} - \bar{\boldsymbol{p}}\|_{\boldsymbol{m}}^\infty\colon \boldsymbol{g}_j(\boldsymbol{p}, \boldsymbol{d}) = 0\right\} \tag{20}$$

Hence, the critical parameter value problem is solved for each individual constraint function, and the answer is selected that is closest to the designated point in the $\boldsymbol{m}$-scaled infinity norm. The reader should realize the similarities among the sets of Eqs. (6–8), (14–16), and (18–20). Rewriting this using the definition of the $\boldsymbol{m}$-scaled infinity norm gives

$$\tilde{\boldsymbol{p}}^{\,j} = \operatorname{argmin}_{\boldsymbol{p}}\left\{\max_{1 \leq k \leq \dim(\boldsymbol{p})} \frac{|\boldsymbol{p}_k - \bar{\boldsymbol{p}}_k|}{\boldsymbol{m}_k}\colon \boldsymbol{g}_j(\boldsymbol{p}, \boldsymbol{d}) = 0\right\} \tag{21}$$

The max can be eliminated and the objective function made differentiable by introducing the similitude ratio α defined earlier:

$$\langle \tilde{\boldsymbol{p}}^j, \tilde{\alpha}^j \rangle = \operatorname{argmin}_{\boldsymbol{p},\alpha}\{\alpha\colon \boldsymbol{g}_j(\boldsymbol{p}, \boldsymbol{d}) = 0, -\alpha\boldsymbol{m} \leq \boldsymbol{p} - \bar{\boldsymbol{p}} \leq \alpha\boldsymbol{m}\} \tag{22}$$

This eliminates nondifferentiabilities in the objective function. As before, the constraint $\boldsymbol{g}_j = 0$ can be replaced by $\boldsymbol{g}_j \geq 0$. For a fixed $\boldsymbol{d}$, if i is given by Eq. (19) and $\tilde{\alpha} = \tilde{\alpha}^i$, then $\tilde{\boldsymbol{p}} = \tilde{\boldsymbol{p}}^i$ is the critical parameter value and $R_p(\bar{\boldsymbol{p}}, \tilde{\alpha}\boldsymbol{m})$ is the largest hyperrectangle proportional to $R_p(\bar{\boldsymbol{p}}, \boldsymbol{m})$, which fits inside the nonfailure region of the $\boldsymbol{p}$ space. Another interpretation is that $\tilde{\alpha}$ is the radius of the largest unit sphere (in the $\boldsymbol{m}$-scaled infinity norm metric) centered at $\bar{\boldsymbol{p}}$, which fits inside the $\boldsymbol{p}$ space feasible set for the given design $\boldsymbol{d}$.

With these concepts at hand, a robustness test for hyperrectangular support sets is formulated as follows:

Q-test: The design $\boldsymbol{d}$ satisfies the hard constraints prescribed by $\Delta_p = R_p(\bar{\boldsymbol{p}}, \boldsymbol{m})$ and $\boldsymbol{g}(\boldsymbol{p}, \boldsymbol{d}) \leq \boldsymbol{0}$ if and only if $\|Q(\tilde{\boldsymbol{p}})\| \geq 1$. This condition is equivalent to $\|\tilde{\boldsymbol{p}} - \bar{\boldsymbol{p}}\|_{\boldsymbol{m}}^\infty \geq 1$ and to $\rho_R \geq \|\boldsymbol{m}\|$.

Recall that the critical parameter values are $\boldsymbol{p}$ values, not necessarily realizations of $\boldsymbol{p}$, at the verge of violating at least one of the constraints. The robust design space corresponding to $\Delta_p = R_p(\bar{\boldsymbol{p}}, \boldsymbol{m})$ is given by $\{\boldsymbol{d}\colon \rho_R \geq \|\boldsymbol{m}\|\}$, for which the boundary is the iso-rectangular PSM manifold $\rho_R(\boldsymbol{d}) = \|\boldsymbol{m}\|$.

C. Bounding Sets

We next look at how the techniques developed so far can be leveraged to provide robustness tests for support sets with other geometries. The preceding tests and margins enable a rigorous assessment of hyperspherical and hyperrectangular sets. In this section, we use these geometries as bounding sets of support sets having arbitrary shapes. Studies on the bounding sets will be used to infer properties of the support set. Conservatism is unavoidably introduced because the design requirements apply to the actual support set, not to the bounding set.

Bounding test: Let the support set Δ_p be of arbitrary shape. Define an outer bounding set O_p as one satisfying $\Delta_p \subseteq O_p$. If the design $\boldsymbol{d}$ satisfies the hard constraints for the bounding set O_p, the design $\boldsymbol{d}$ satisfies the hard constraints for Δ_p; that is, the design is robust. On the other hand, if the design $\boldsymbol{d}$ does not satisfy the hard constraints for as much as one realization $\boldsymbol{p} \in \Delta_p$, the design $\boldsymbol{d}$ does not satisfy the hard constraints for Δ_p; that is, the design is not robust.

The P- and the Q-tests can be used to determine the robustness of hyperspherical and hyperrectangular bounding sets. Obviously, conservatism is reduced by using tighter bounding sets. Constraint violations caused by parameter values falling inside O_p but outside of Δ_p might cause a robust design to fail the bounding test. Conservative approximations to the robust design space for arbitrarily shaped support sets can be easily calculated using PSMs. For instance, if $O_p = S_p(\bar{\boldsymbol{p}}, R)$, the design set $\{\boldsymbol{d}\colon \rho_S \geq R\}$ is a subset of the actual robust design space.

The P- and Q-tests are applicable to multidimensional support sets having hyperspherical and hyperrectangular shapes. The bounding test, which is based on these two tests, is applicable to support sets having an arbitrary geometry. As such, this suite of tools is not restricted by the geometry of the uncertainty set or its dimension, and as a result, it is widely applicable.

D. Designs Outside the Feasible Design Space

Thus far we have only considered the case in which the designated point is in the feasible design space. The case when the designated point is in the infeasible region [i.e., $\boldsymbol{g}(\bar{\boldsymbol{p}}, \boldsymbol{d}) \not\leq \boldsymbol{0}$] is introduced next. One situation in which a need for this extension might arise is if an automated optimization-driven design procedure varies the design parameter so much that constraint boundaries move enough to make $\bar{\boldsymbol{p}}$ a constraint violation point. If $\bar{\boldsymbol{p}} \in F^c$ (where the superscript c denotes the set complement operator), the critical parameter value for hyperspherical support sets is given by

$$\begin{aligned}\tilde{\boldsymbol{p}} &= \text{argmin}_{\boldsymbol{p}}\{\|\boldsymbol{p} - \bar{\boldsymbol{p}}\|\colon \boldsymbol{p} \in F^c\} \\ &= \text{argmin}_{\boldsymbol{p}}\{\|\boldsymbol{p} - \bar{\boldsymbol{p}}\|\colon \boldsymbol{g}_i(\boldsymbol{p}, \boldsymbol{d}) \leq 0, 1 \leq i \leq \dim(\boldsymbol{g})\}\end{aligned} \tag{23}$$

Expressions for hyperrectangular support sets are obtained by using $\|Q(\boldsymbol{p})\|$ instead of $\|\boldsymbol{p} - \bar{\boldsymbol{p}}\|$ in Eq. (23). Recall that designs outside the feasible design space will have negative PSMs.

E. Discussion

The methods presented in this paper are applicable when constraint feasibility is desired (i.e., all the members of the uncertainty model satisfy the constraints). In this case, if an arbitrary probability density function is defined over the support set, the probability of failure is zero. Evaluating a probability of zero is difficult for most of the methods available, including tools for handling soft constraints [1,5,10,12–15]. For instance, even though a Monte Carlo approximation to this probability will always be zero, one will never know if such a number is a consequence of using a finite number of samples. Because the accuracy of the Monte Carlo approximation degrades as the probabilities get smaller, one may believe that hard constraints are feasible when a subset of the uncertainty model violates the constraints with small probability. If optimization-based methods such as the first- and second-order reliability methods (FORM and SORM) [3] are used to approximate the aforementioned probability, these methods will not converge. This is so, because the constraint violation set is empty; thus, its corresponding boundary (i.e., the limit state surface) is also empty. The tools derived herein allow determination of whether there are constraints violations at all. Therefore, the present tools complement other uncertainty propagation tools when those other tools are inapplicable or inaccurate, a situation that arises when the design objectives are actually met.

At this point, it is important to highlight some major differences between the methods developed here and the ones conventionally used for uncertainty propagation.

The prescription of probabilistic uncertainty models entails setting not only the support set, but also a probability density function within the set, information that requires knowledge of the frequency in which events within the set occur. In contrast to these models, the models used in this paper only require prescribing the designated point and the relative levels of uncertainty among the uncertain parameters. The designated point, which is our best single estimate of the uncertain parameter, is comparatively simple to model. Although conventional methods require prescribing fixed absolute ranges of variation for each uncertain parameter (e.g., Δ_{p_1} and Δ_{p_2}), the developments proposed herein only require knowing how those ranges relate among themselves (e.g., $|\Delta_{p_1}|/|\Delta_{p_2}|$). Hence, the shape, but not the size, of the support set being deformed determines the size of the maximal feasible set.

Notice also that the robustness assessments resulting from the strategies proposed are more general than those used by conventional approaches. For instance, assume that there is a probabilistic uncertainty model for which the support set captures deviations from the designated point of up to 5% in each individual component. If the propagation of this set through $\boldsymbol{g}$ using conventional approaches leads to a failure probability of zero, one will not know if the same outcome is obtained for variations of up to 6%. Using the methods presented here, the deformation of the support set enables the determination of the largest variation for which hard constraints are satisfied (i.e., the largest variations for which zero failure probability is still attained). For any uncertainty model, probabilistic or not, for which the support fits within the largest variation box, we will know that the failure probability is zero without further computations.

V. Robust Design

Problem Statement: For a given support set Δ_p and a set of constraints, find the design $\boldsymbol{d}^*$ with the best robustness characteristics.

In the context of this paper, this statement is addressed by searching for the design point that maximizes the PSM. This is implemented as follows:

$$\boldsymbol{d}^* = \text{argmax}_{\boldsymbol{d}}\{\tilde{\alpha}(\bar{\boldsymbol{p}}, \Delta_p, \boldsymbol{d}, \boldsymbol{g})\} \tag{24}$$

The corresponding maximum feasible set depends on Δ_p, $\bar{\boldsymbol{p}}$, and the critical similitude ratio corresponding to $\boldsymbol{d}^*$. Design strategies for hyperspherical and hyperrectangular support sets are presented next. The former case will be referred to as the P-search and the latter one as the Q-search.

In general, this problem may not have a unique solution unless restrictions [6,15] on the way in which $\boldsymbol{g}$ depends on $\boldsymbol{p}$ apply. In addition, it may be that for some designs $\boldsymbol{d}$, there are no values of the parameter $\boldsymbol{p}$ leading to constraint violations. These designs lead to an unbounded M and maximal robustness to parameter uncertainty, as defined in the present context.

P-search: If $\boldsymbol{g} \leq \boldsymbol{0}$ is a set of constraints and $S_p(\bar{\boldsymbol{p}}, R)$ is the support set, a design with the best robustness characteristics (namely, $\boldsymbol{d}^S$) and the corresponding maximum feasible set are given by

$$\boldsymbol{d}^S = \text{argmin}_{\boldsymbol{d}}\{-\rho_S(\bar{\boldsymbol{p}}, \tilde{\boldsymbol{p}}, \boldsymbol{d})\} \tag{25}$$

$$\mathcal{M} = S_p(\bar{\boldsymbol{p}}, \rho_S(\bar{\boldsymbol{p}}, \tilde{\boldsymbol{p}}, \boldsymbol{d}^S)) \tag{26}$$

Q-search: If $\boldsymbol{g} \leq \boldsymbol{0}$ is a set of constraints and $R_p(\bar{\boldsymbol{p}}, \boldsymbol{m})$ is the support set, a design with the best robustness characteristics (namely,

$\boldsymbol{d}^R$) and the corresponding maximum feasible set are given by

$$\boldsymbol{d}^R = \text{argmin}_{\boldsymbol{d}}\{-\rho_R(\bar{\boldsymbol{p}}, \tilde{\boldsymbol{p}}, \boldsymbol{m}, \boldsymbol{d})\} \tag{27}$$

$$M = R_p\left(\bar{\boldsymbol{p}}, \frac{\rho_R(\bar{\boldsymbol{p}}, \tilde{\boldsymbol{p}}, \boldsymbol{m}, \boldsymbol{d}^R)\boldsymbol{m}}{\|\boldsymbol{m}\|}\right) \tag{28}$$

Note that $-\|Q(\tilde{\boldsymbol{p}})\|$ can also be used as the objective of the optimization problem in Eq. (27). Details on the derivation of Eq. (28) and on the existence of the robust design space are available [21] in the literature.

Sizing M is an important task in reliability-based design optimization. Probabilistic techniques, typically used to handle soft inequality constraints, should not be used when the support set of the probability density function of the uncertain parameter is a subset of $\mathcal{M}$. Otherwise, numerical error might lead to the false identification of robust designs.

A. Discussion

Traditionally, when one encounters the combination of the notions of "design" and "optimization", one thinks in terms of optimizing an objective function that quantifies some measure of the performance of the system being designed. Note that in the present context, it is robustness, not performance, that is being optimized. However, traditional measures of performance can be incorporated into the present paradigm by incorporating fixed levels of desired performance in the constraint functions. Once constraint levels have been set and a robust design has been found, the designer can iterate the process by changing the constraint levels on those constraints to see if better performance can be achieved while preserving robustness. In this way, tradeoffs between robustness and performance can be studied. If $\boldsymbol{g}$ has conflicting design requirements, the robust design strategies of this section will lead to compromises in robustness, in which optimal tradeoffs are naturally reached.

VI. Examples

The methods and tools proposed herein are applicable to realistic engineering problems, which are generally multidimensional and nonlinear and for which explicit expressions for the design constraints are usually unavailable. However, the examples presented next have been chosen to enable the visualization and reproducibility of the results.

A. Two-Dimensional Example

A two-dimensional problem in the design variables (i.e., $\boldsymbol{d} = [\boldsymbol{d}_1, \boldsymbol{d}_2]^T$) and in the uncertain parameter (i.e., $\boldsymbol{p} = [\boldsymbol{p}_1, \boldsymbol{p}_2]^T$) is considered here. Let the set of constraints be prescribed by

$$\boldsymbol{g}_1 = 3\boldsymbol{d}_2 - 4\boldsymbol{p}_1^2 - 4\boldsymbol{d}_1\boldsymbol{p}_2 \sin\left(\boldsymbol{p}_2\boldsymbol{d}_1 - \boldsymbol{p}_1^2\right) \tag{29}$$

$$\boldsymbol{g}_2 = -\sin\left[\boldsymbol{p}_1^2\boldsymbol{p}_2 - \sin(2\boldsymbol{p}_1 - 2)\right] - \boldsymbol{d}_1\boldsymbol{d}_2\boldsymbol{p}_1 - \boldsymbol{p}_2 \tag{30}$$

$$\boldsymbol{g}_3 = \boldsymbol{d}_1 + \boldsymbol{p}_1^2\boldsymbol{d}_2^2 - 4\boldsymbol{p}_2^2\boldsymbol{p}_1 - 4\sin(2\boldsymbol{p}_1 - 2\boldsymbol{p}_2) \tag{31}$$

$$\boldsymbol{g}_4 = 2(\boldsymbol{p}_1 + \boldsymbol{p}_2)\sin\left(\boldsymbol{p}_1^2 - \boldsymbol{d}_2\right) - 2\boldsymbol{p}_1\boldsymbol{p}_2\left(\boldsymbol{d}_2 + 2\boldsymbol{p}_1^2 - 2\right) + \boldsymbol{d}_1 - 6\boldsymbol{p}_1 \tag{32}$$

and the designated point be $\bar{\boldsymbol{p}} = [1, 1]^T$. The contour of the corresponding feasible design space is marked with a solid thick line in subsequent figures.

The first analysis of this example will make use of a hyperspherical support set (a circle in this two-dimensional example) Δ_p, centered at $\bar{\boldsymbol{p}}$. This choice of support set might indicate the analyst's judgment that the uncertainty in the uncertain parameter is geometrical in nature, with no distinctions made based on the direction of perturbation from the designated point. The function $\rho_S(\boldsymbol{d})$ for design points in the feasible design space is shown in Fig. 3. Recall that for a given design point, its PSM is the size of the largest perturbation to $\bar{\boldsymbol{p}}$ allowed before a constraint is violated. For ease of comparability, the color scale used in Fig. 3 is the same as that in subsequent figures. This figure illustrates that the design with the best robustness characteristics is able to tolerate uncertainty in $\boldsymbol{p} = \bar{\boldsymbol{p}} + \boldsymbol{u}$ with $\|\boldsymbol{u}\| \leq 0.53$. Therefore, variations of less than 0.53 lead to nonempty robust design spaces. The boundary of the feasible design space is given by the $\rho_S(\boldsymbol{d}) = 0$ contour. Notice that multiple PSM maxima occur (there are local maxima in the vicinity of $[-1, 0]^T$ and of $[-2.2, -2.4]^T$). More important, notice that designs further in from the boundary of the feasible design space are not necessarily more robust. This fact is counterintuitive and is a result of the PSM of a given design point depending on how far the constraint boundaries for that design point are from the designated point, and the distance of the design point from the feasible design space boundary is related to the gradient phenomenon of how rapidly the constraint boundaries move (toward the designated point) as the design point is altered. For instance, the comparison of $\boldsymbol{d1} = [-2.25, -2.4]^T$ (marked in Fig. 3 with the circle symbol) and $\boldsymbol{d2} = [-1, -1]^T$ (marked in Fig. 3 with the square symbol) shows that $\rho_S(\boldsymbol{d1}) \gg \rho_S(\boldsymbol{d2})$, even though $\boldsymbol{d1}$ is much closer to the boundary of the feasible design space than $\boldsymbol{d2}$.

Now we consider the hyperrectangular support set $\Delta_p = R_p(\bar{\boldsymbol{p}}, \boldsymbol{m1})$, where $\boldsymbol{m1} = [1, 1]^T$ (so, in this two-dimensional example, Δ_p is a square). This choice of support set might indicate the analyst's judgment that the uncertainties in the components of the uncertain parameter are independent of each other, but of about the same magnitude. The corresponding rectangular PSM function is shown in Fig. 4. Larger margins are now attained. Similarities in the distribution of PSMs arise because the offsets between the circles (i.e., two-dimensional hyperspheres) and the squares (i.e., two-dimensional regular hyperrectangles) used are relatively small.

Figure 5 shows the rectangular PSM function for $R_p(\bar{\boldsymbol{p}}, \boldsymbol{m2})$ where $\boldsymbol{m2} = [1, 4]^T$. This choice of support set might indicate the analyst's judgment that the uncertainties in the components of the uncertain parameter are independent of each other and that the level of uncertainty in the second component is about four times that of the first. Considerable differences in the distribution and magnitude of the PSMs, when compared with the previous two figures, are apparent. These differences will be discussed further when design tools are applied in this example.

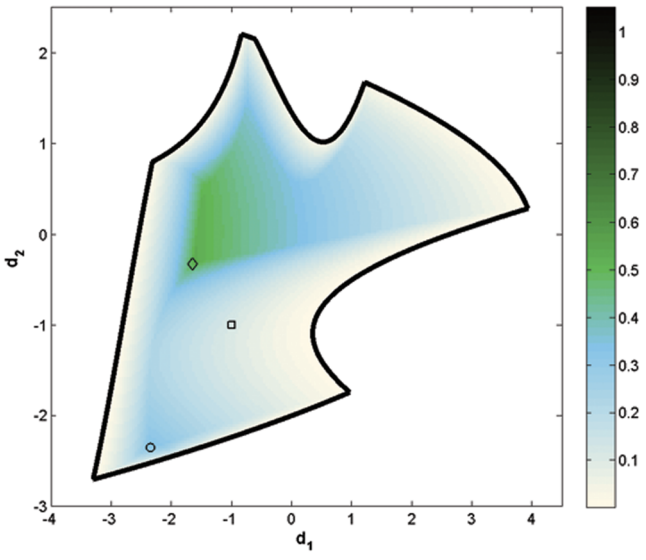

Fig. 3 Spherical PSMs. The most robust design $\boldsymbol{d}^S$ is marked as a diamond.

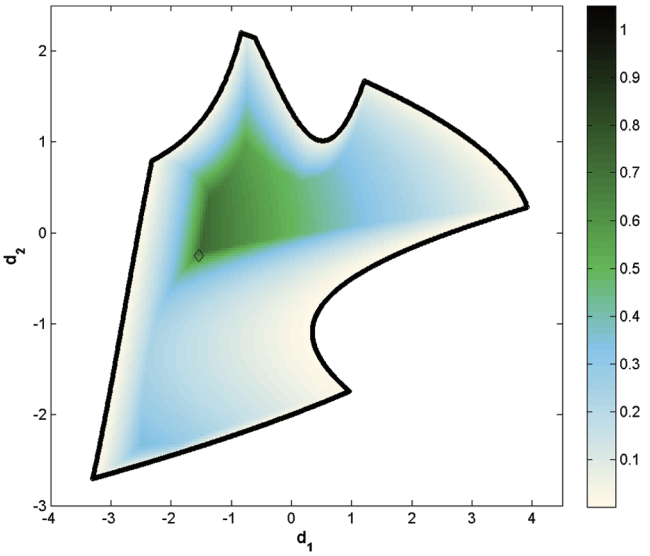

Fig. 4 Rectangular PSMs for $\mathcal{R}(\bar{p}, m1)$. The most robust design d^R is marked as a diamond.

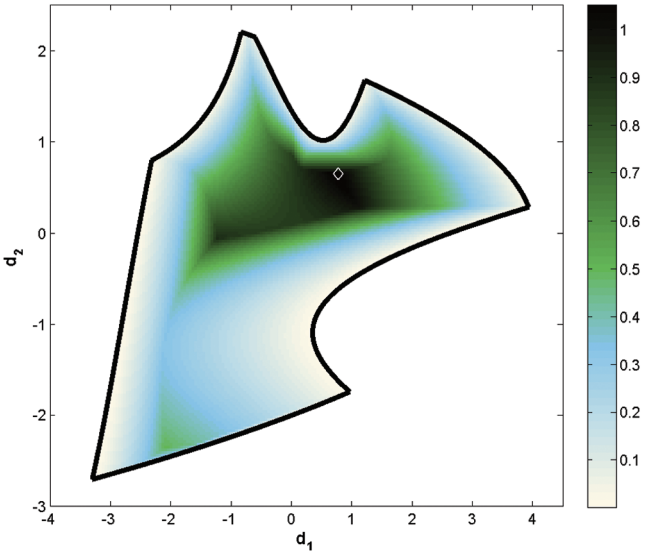

Fig. 5 Rectangular PSMs for $\mathcal{R}(\bar{p}, m2)$.

An application of the material of Sec. IV.C on bounding sets is now presented. Consider the triangular support set shown in the left of Fig. 6 in light gray. The tightest bounding circle and rectangle are superimposed. Clearly, the rectangle better approximates the triangular set. The robust design spaces corresponding to both bounding sets, calculated via spherical PSMs and rectangular PSMs, are shown in the right subplot of Fig. 6. For purposes of display only, all robust design space plots are based on discretizing $\boldsymbol{d}$ over a grid of 201 by 201 points from the rectangle $[-4, 5] \times [-3.5, 2.5]$. The robust design space for the bounding circle is filled in with black and the robust design space for the bounding rectangle is colored in dark gray. The robust design space for the rectangle contains the one for the sphere. This is expected, because the hypersphere contains the hyperrectangle, and any design that satisfies all constraints for every value of $\boldsymbol{p}$ in the hypersphere perforce satisfies all constraints for every value of $\boldsymbol{p}$ in the hyperrectangle. The bounding set technique just used to underestimate the robust design space of the triangle was used, because we have no tools comparable with the ones used for hyperspheres and hyperrectangles to determine the exact robust design space for the triangle. To get an approximation of this true robust design space, we apply a sampling technique. A sample set of 200,000 $\boldsymbol{p}$ points is generated in the triangle so that it is distributed

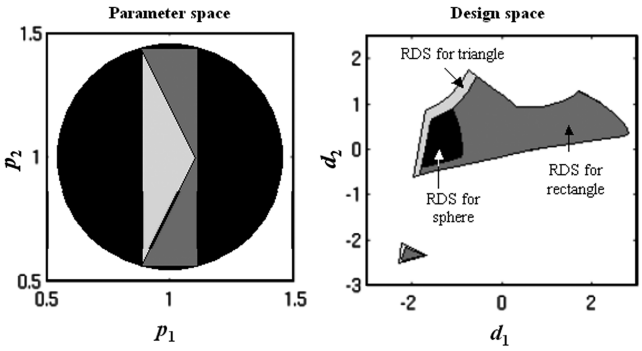

Fig. 6 Triangular support set and outer bounding sets (left) and corresponding robust design space approximations (right).

evenly over the triangular area. A point $\boldsymbol{d}$ in the design space grid is deemed to be in the robust design space of the triangle if, for this $\boldsymbol{d}$, all constraints are satisfied at every one of the 200,000 sample points from the triangle. We have high confidence that a point passing this test is in the robust design space of the triangle, but this is not certain. Such a computationally intensive analysis is only feasible in such a simple problem as is considered in this example. The corresponding robust design space approximation is colored with light gray in Fig. 6. The bounding-based approximations are both subsets of the sampling-based approximation. The conservatism introduced by using the bounding circle leads to a considerably smaller robust design space approximation. Note that the portion of the robust design space in the vicinity of $\boldsymbol{d} = [-2, -2.25]^T$ is completely omitted by the circular approximation. The robust design space corresponding to the rectangle is a better approximation, because the offset between the rectangle and the triangle is smaller. The conservatism introduced by bounding might lead to an empty approximation of the robust design space, even though the actual robust design space is nonempty. Notice, however, that although the sampling-based robust design space approximation is the largest, only the approximations resulting from the bounding sets are reliable. This is so, because when the support set is a hypersphere or a hyperrectangle, it can be determined unequivocally whether a given design point is in the robust design space or not.

The tools of Sec. V for robust design are used next. Although the search for the design with best robustness characteristics corresponding to a circular support leads to $\boldsymbol{d}^S = [-1.65, -0.33]^T$ and $M = S_p(\bar{\boldsymbol{p}}, 0.53)$, the one corresponding to the rectangular support set $R_p(\bar{\boldsymbol{p}}, \boldsymbol{m2})$ leads to $\boldsymbol{d}^R = [0.718, 0.631]^T$ and $M = R_p(\bar{\boldsymbol{p}}, 0.26\boldsymbol{m2})$. The optimal designs are marked with diamonds in Figs. 3–5. There is a strong dependence of the robustness on the geometry of the support set. The knowledge available (or the lack of it) of the uncertainty in the uncertain parameters determines the geometry of the uncertainty set, and such a set determines not only the PSM associated with any given design point but also the most robust design overall. For instance, although the support sets used in Fig. 3 and 4 imply that the uncertainties in $\boldsymbol{p}1$ and $\boldsymbol{p}2$ are comparable, the support used in Fig. 5 implies that there is four times more certainty in the value of $\boldsymbol{p}1$ relative to the one in $\boldsymbol{p}2$. This change leads to a different PSM distribution and to a different location of the most robust design (i.e., the most robust design transitions from $[-1.65, -0.33]$ to $[0.718, 0.631]$). This comparison illustrates how the refinement of the uncertainty model, say through more experiments or additional simulations, impacts the selection of the optimal design. These sets are shown in Figs. 7 and 8, along with the corresponding critical parameter values.

Note that changing the design point has altered the constraint boundaries. Three critical parameter values exist in both cases. This situation arises because there are conflicting design objectives in $\boldsymbol{g}$, so when one tries to move the boundary of a given constraint away from the designated point, the boundary of another one gets closer. Design optimization may lead to maximal feasible sets with multiple critical parameter values, such as those shown, when a compromise in the robustness of conflicting design objectives is attained.

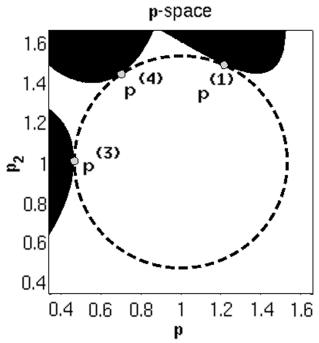

Fig. 7 Maximum feasible set.

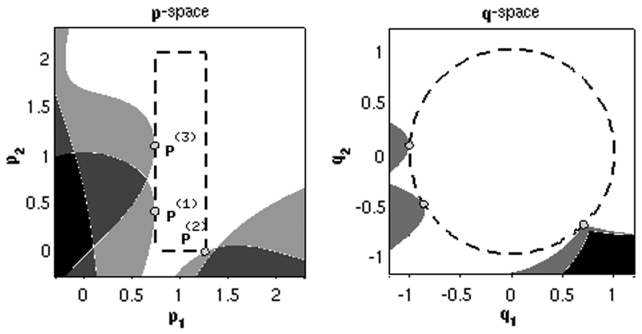

Fig. 8 Maximum feasible set proportional to $R(\bar{p}, m2)$ (left) and corresponding set in q space (right).

B. Flutter-Speed Analysis

In this example, we study the stability in flutter of the simple aeroelastic wing model shown in Fig. 9. Supporting information is found in work of Bisplinghoff et al. [26].

The uncertain parameters in this study are two aerodynamic derivatives and the bending and torsional stiffness of the wing. For purposes of uncertainty analysis, the freestream velocity and the distance of the movable mass m_2 from the aeroelastic axis are considered to be the design variables. The system requirement is that the wing be stable in flutter. This translates into constraints that the four eigenvalues of the linearized system lie in the left half-plane. Ultimately, the analysis information will be used to schedule the position of the movable mass as a function of freestream velocity so that, at each velocity, the system is as robust (in the sense of spherical PSMs or rectangular PSMs) in flutter as possible.

The aerodynamic forces and moments are applied at the quarter-chord point of the wing; the location of the center of gravity of the system can be adjusted by changing the distance d between the movable mass m_2 and the elastic axis A. The linearized equations of motion are given by

$$\begin{bmatrix} \dot{\boldsymbol{x}} \\ \ddot{\boldsymbol{x}} \end{bmatrix} = \begin{bmatrix} \mathbf{0} & \mathbf{I} \\ -\mathbf{M}^{-1}\mathbf{K} & -\mathbf{M}^{-1}\mathbf{C} \end{bmatrix} \begin{bmatrix} \boldsymbol{x} \\ \dot{\boldsymbol{x}} \end{bmatrix} \tag{33}$$

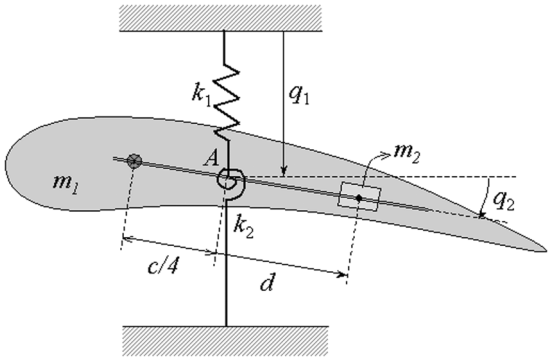

Fig. 9 Two-degree-of-freedom flutter model.

where $\boldsymbol{x} = [q_1, q_2]^T$ is the state-space vector and

$$\mathbf{M} = \begin{bmatrix} m_1 + m_2 & m_1 l + m_2 d \\ m_1 l + m_2 d & I_A + m_2 d^2 \end{bmatrix} \tag{34}$$

$$\mathbf{C} = qs \begin{bmatrix} C_{l_\alpha}/4 & 0 \\ -cC_{l_\alpha}/(4u) & -cC_{m_\alpha} \end{bmatrix} \tag{35}$$

$$\mathbf{K} = \begin{bmatrix} k_1 & qsC_{l_\alpha} \\ 0 & k_2 - qscC_{l_\alpha}/4 \end{bmatrix} \tag{36}$$

In these expressions, m_1 is the mass of the wing, l is the distance between A and the center of gravity of the wing, c is the cord length, s is the wing's reference area, I_A is the moment of inertia of the wing about A, q is the dynamic pressure, u is the freestream velocity, C_{l_α} and C_{m_α} are stability derivatives, and k_1 and k_2 are the bending and torsional stiffnesses, respectively. For simplicity, we have assumed that d varies slowly enough to neglect the Coriolis effect.

The following numerical values are assumed: $m_1 = 0.5$ kg, $m_2 = 0.5$ kg, $l = 0.1$ m, $I_A = 0.1$ kgm^2, $q = 0.6125u^2$ kg/m^3, $s = 1$ m^2, and $c = 1$ m. The parameters C_{l_α}, C_{m_α}, k_1, and k_2 are considered uncertain. A nondimensional $\boldsymbol{p}$ space is obtained by using the parametrization

$$[C_{l_\alpha}, C_{m_\alpha}, k_1, k_2]^T = \text{diag}\{[2\pi, 0, 6 \times 10^5, 10^5]\}\boldsymbol{p} + \text{diag}\{[0, 0.01, 0, 0]\}(\boldsymbol{p} - \bar{\boldsymbol{p}}) \tag{37}$$

where $\bar{\boldsymbol{p}} = [1, 1, 1, 1]^T$. Design requirements for flutter speed are given by the set of constraints $\boldsymbol{g}_i = Re\{\lambda^{(i)}\}/\|\lambda^{(i)}\|$ for $i = 1, \ldots, 4$, where $\lambda^{(i)}$ is the ith eigenvalue of the matrix in Eq. (33).

In this example, the feasible design space is given by the $\langle u, d \rangle$ pairs for which the system is stable when $\boldsymbol{p} = \bar{\boldsymbol{p}}$. The distribution of spherical PSMs in the feasible design space is shown in Fig. 10. The position of the moving mass that maximizes the spherical PSM at each particular u is indicated by the dotted line. Once the pair $\langle u, d \rangle$ is fixed, we can deform the support set until a point on the boundary of the failure domain $\boldsymbol{g} = 0$ is reached. When this domain is reached, the system becomes unstable. In our calculations, we sweep the range of interest for u, and at each speed, we solve for the value of d that maximizes the PSM. The collection of d values leads to the trail shown in Fig. 10.

Deformations of the hyperrectangle centered at $\bar{\boldsymbol{p}}$ with $\boldsymbol{m} = [20, 4, 5, 10]$ lead to Fig. 11. As before, the most robust positions of the moving mass are indicated by the dotted line. The discontinuity in the d schedule as a function of u is not necessarily a reflection of any discontinuities in the rectangular PSM. Instead, it reflects the shape

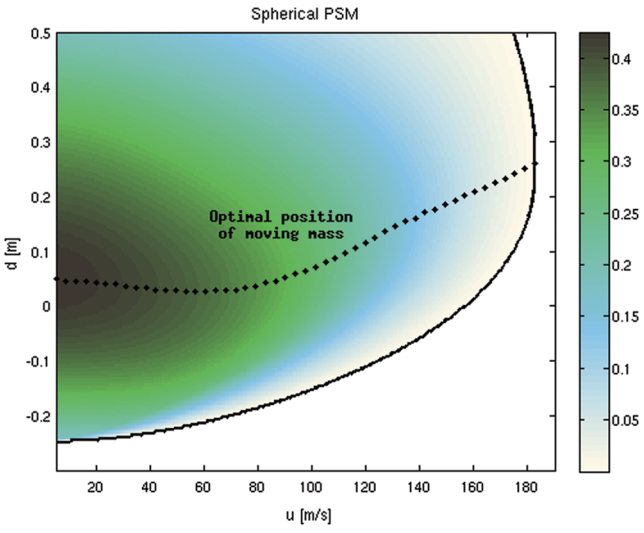

Fig. 10 Spherical PSMs in the nominally stable $\langle u, d \rangle$ space.

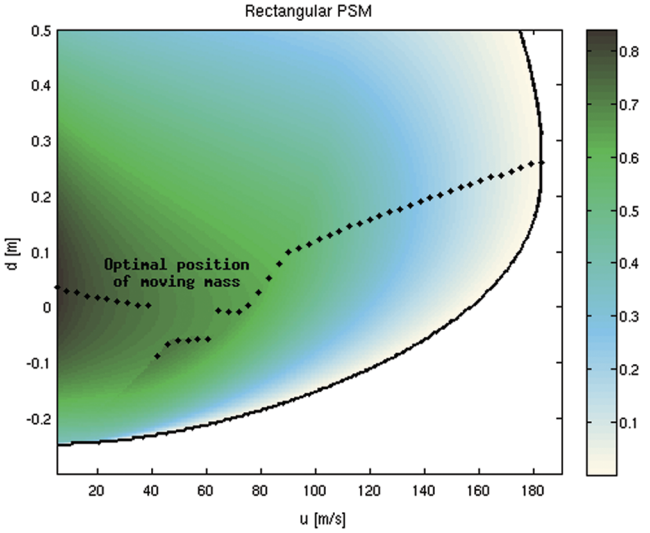

Fig. 11 Rectangular PSMs in the nominally stable $\langle u, d \rangle$ space.

of the PSM surface. This surface has a major high point on the left edge of the plot and a local maximum near $\langle u, d \rangle = \langle 48, -0.06 \rangle$. These are separated by a "valley." The schedule of d as a function of u is calculated by moving u from left to right and, at each value of u, finding the maximum PSM value over all feasible d. The point (actually, a point: there might be more than one) at which that maximum occurs is marked by a dot on the dotted line. As u moves from left to right, this location jumps over the valley at two different u values, creating the discontinuities in the curve. The comparison of Figs. 10 and 11 indicates the sensitivity of the robustness metrics to the geometry of the uncertainty model.

VII. Conclusions

A methodology for robustness analysis and robust design of systems subject to parametric uncertainty was proposed. Emphasis was given to uncertainty sets prescribed or bounded by hyperspheres or hyperrectangles. The tools developed herein enable the exploration of the targeted regions of the design space in which the design requirements are satisfied for all members of the uncertainty set. Formal assessments of robustness are possible because these sets lend themselves to a rigorous mathematical treatment for which sampling/partitioning the parameter space is not required. The present tools are applicable in cases in which traditional techniques (sampling, FORM, etc.) fail. With traditional techniques, if the uncertainty model is changed, the uncertainty analysis must be redone. With the present tools, once a maximal feasible set is calculated, if a new uncertainty model is considered that still falls within the maximal feasible set, conclusions may be drawn about robustness of the system without the calculational expense of additional system simulations. The ideas proposed here are general and not discipline-dependent, making them applicable to a broad spectrum of engineering problems.

References

[1] Kall, P., and Wallace, S., *Stochastic Programming*, Wiley, New York, 1994.

[2] Ermoliev, Y., "Stochastic Quasigradient Methods and Their Applications to Systems Optimization," *Stochastics*, Vol. 9, No. 1, 1983, pp. 1–36.

[3] Rackwitz, R., "Reliability Analysis, a Review and Some Perspectives," *Structural Safety*, Vol. 23, No. 4, 2001, pp. 365–395. doi:10.1016/S0167-4730(02)00009-7

[4] Luis, R. M., Teixeira, A. P., and Soares, C. G., "Longitudinal Strength Reliability of a Tanker Accidentally Grounded," *European Safety and Reliability Conference*, Vol. 2, Taylor and Francis, London, 18–22 Sept. 2006, pp. 1499–1509.

[5] Crespo, L. G., and Kenny, S. P., "Reliability-Based Control Design for Uncertain Systems," *Journal of Guidance, Control, and Dynamics*, Vol. 28, No. 4, 2005, pp. 649–658.

[6] Darlington, J., Pantelides, C., Rustem, B., and Tanyi, B., "An Algorithm for Constrained Nonlinear Optimization Under Uncertainty," *Automatica*, Vol. 35, No. 2, 1999, pp. 217–228. doi:10.1016/S0005-1098(98)00150-2

[7] Mulvey, J. N., Vanderbrei, R. J., and Zenios, S. A., "Robust Optimization of Large Scale Systems," *Operations Research*, Vol. 2, No. 43, 1995, pp. 264–280.

[8] Gustafson, S. A., *Semi-Infinite Programming and Applications*, Springer, Berlin, 1981.

[9] Howe, M. A., Rustem, B., and Selby, M. J. P., "Multi-Period Minimax Hedging Strategies," *European Journal of Operational Research*, Vol. 1, No. 93, 1996, pp. 185–204.

[10] Rustem, B., and Nguyen, Q., "An Algorithm for the Inequality Constrained Minimax Problem," *SIAM Journal on Optimization*, Vol. 8, No. 1, 1998, pp. 265–283. doi:10.1137/S1056263493260386

[11] Tenne, D., and Singh, T., "Efficient Minimax Control Design for Prescribed Parameter Uncertainty," *Journal of Guidance, Control, and Dynamics*, Vol. 27, No. 6, 2004, pp. 1009–1016.

[12] Engelund, S., and Rackwitz, R., "A Benchmark Study of Importance Sampling Techniques in Structural Reliability," *Structural Safety*, Vol. 12, No. 4, 1993, pp. 255–276. doi:10.1016/0167-4730(93)90056-7

[13] Mahadevan, S., and Raghothamachar, P., "Adaptive Simulation for System Reliability Analysis of Large Structures," *Computers and Structures*, Vol. 77, No. 6, 2000, pp. 725–734. doi:10.1016/S0045-7949(00)00013-4

[14] Robinson, D., and Atcitty, C., "Comparison of Quasi- and Pseudo-Monte Carlo Sampling for Reliability and Uncertainty Analysis," *AIAA Structures, Structural Dynamics and Materials Conference*, Vol. 1, AIAA, Reston, VA, 1999, pp. 2942–2949; also AIAA Paper 1999-1589, 1999.

[15] Royset, J., Kiureghian, A. D., and Polak, E., "Reliability-Based Optimal Structural Design by the Decoupling Approach," *Reliability Engineering and System Safety*, Vol. 73, No. 3, 2001, pp. 213–221.

[16] Rangavajhala, S., Mullur, A., and Messac, A., "The Challenge of Equality Constraints in Robust Design Optimization: Examination and New Approach," *Structural and Multidisciplinary Optimization*, Vol. 34, No. 5, Nov. 2007, pp. 381–401. doi:10.1007/s00158-007-0104-8

[17] Fares, B., Noll, D., and Apkarian, P., "Robust Control via Sequential Semi Definite Programming," *SIAM Journal on Control and Optimization*, Vol. 40, No. 6, 2002, pp. 1791–1820. doi:10.1137/S0363012900373483

[18] Allen, J. K., Seepersad, C., Choi, H., and Mistree, F., "Robust Design for Multiscale and Multidisciplinary Applications," *Journal of Mechanical Design*, Vol. 128, 2006, pp. 832–843. doi:10.1115/1.2202880

[19] Mourelatos, Z. P., and Liang, J., "A Methodology for Trading-Off Performance and Robustness Under Uncertainty," *Journal of Mechanical Design*, Vol. 128, 2006, pp. 856–863. doi:10.1115/1.2202883

[20] Das, I., "Robust Optimization for Constrained, Nonlinear Programming Problems," *Engineering optimization*, Vol. 32, No. 5, 2000, pp. 585–618. doi:10.1080/03052150008941314

[21] Crespo, L. G., Giesy, D. P., and Kenny, S. P., "Strict Feasibility in Optimization under Uncertainty," 11th AIAA/ISSMO Multidisciplinary Analysis and Optimization Conference, Portsmouth, VA, AIAA Paper 2006-7035, Sept. 2006.

[22] Crespo, L. G., Giesy, D. P., and Kenny, S. P., "Reliability-Based Analysis and Design via Failure Domain Bounding," *Structural Safety* (submitted for publication).

[23] Ben-Haim, Y., *Info-Gap Decision Theory: Decisions Under Severe Uncertainty*, 2nd ed., Academic Press, London, 2006.

[24] Ben-Haim, Y., "A Non-Probabilistic Measure of Reliability of Linear Systems Based on Expansion of Convex Models," *Structural Safety*, Vol. 17, No. 2, 1995, pp. 91–109. doi:10.1016/0167-4730(95)00004-N

[25] Ben-Haim, Y., "Uncertainty, Probability and Information-Gaps," *Reliability Engineering and System Safety*, Vol. 85, 2004, pp. 249–266.

[26] Bisplinghoff, R. L., Ashley, H., and Halfman, R. L., *Aeroelasticity*, Addison–Wesley, New York, 1955; republished, Dover, Mineola, NY, 1996.

A. Messac
Associate Editor